Characterisation and Cancellation of Interference with Multiple Phase-coded FMCW Dual-Function RADAR Communication Systems

François De Saint Moulin*, Claude Oestges†, Luc Vandendorpe‡
ICTEAM, UCLouvain - Louvain-la-Neuve, Belgium
*francois.desaintmoulin@uclouvain.be, †claude.oestges@uclouvain.be, ‡luc.vandendorpe@uclouvain.be

2022 IEEE 95th Vehicular Technology Conference (VTC2022-Spring) | 978-1-6654-8243-1/22/$31.00 ©2022 IEEE | DOI: 10.1109/VTC2022-Spring54318.2022.9860642

***Abstract*—In this paper, the impact of interference between multiple phase-coded Frequency Modulated Continuous Wave (FMCW) Dual Function Radar Communication (DFRC) systems is analysed. For the RADAR receiver, interference occurs when another nearby DFRC system is active. For the communication receiver, RADAR echoes from the same DFRC system interfere with the receiver. The performance achieved by interference cancellation at both functions is studied in different scenarios. Finally, stochastic geometry is used to analyse in a two-way automotive scenario which signal component (RADAR or communication) is dominant, in order to evaluate whether the interference should be cancelled at the RADAR receiver based on the communication receiver output or the opposite.**

***Index Terms*—FMCW, DFRC, RADAR, communication, interference, interference cancellation, stochastic geometry**

I. Introduction

In recent years, with the spectrum scarcity and the convergence of the carrier frequency ranges used by RADAR and communication systems, the possibility to operate both functions using the same resources has received an increased attention. Joint RADAR-Communication systems enable to perform both functions simultaneously with a single hardware platform [1]–[3]. Two approaches have been adopted: coexistence and co-design. In the former, different waveforms are used for each function, and interference between both functions must be mitigated. In the latter, a single waveform is transmitted, and trade-offs are made in the waveform design between both functions. These are also often called Dual Function RADAR-Communication (DFRC) systems. Numerous systems have been developed based on existing RADAR waveforms or communication protocols. Among these systems, as a non exhaustive list, popular waveforms are the frequency hopping-based waveforms, Linear Frequency Modulation (LFM)/Frequency Modulated Continuous Wave (FMCW)-based waveforms, or the Orthogonal Frequency Division Multiplexing (OFDM)-based waveforms. In particular, the FMCW waveform is a popular RADAR waveform, widely used in automotive applications thanks to its low complexity and implementation cost. In order to introduce communication capabilities, the good cross-correlation properties of the up- and down-chirps enable to distinguish the transmission of a '0' or a '1', without affecting the RADAR function. This approach is adopted in [4] in association with Alamouti space-time coding. However, the achievable rate is limited by the Pulse Repetition Interval (PRI) with inter-pulse coding. In order to integrate multiple symbols during the pulse duration, [5] has proposed to modulate the FMCW waveform. This has been extended for higher order modulations in [6]–[8] with different designs, and also generalised for a MIMO configuration in [9]. Hardware implementations have been demonstrated in [10]–[12]. Another design based on index modulation involving multiple carrier frequencies and antennas is proposed in [13], [14].

In order to limit distortions induced by phase changes at the power amplifier, Continuous Phase Modulations (CPM) and Minimum Shift Keying (MSK) are introduced to fulfil the communication function in [15], [16], and an experimental setup is shown in [17]. This has also been used in [18] with a MIMO configuration for multiple users. Note that the integration of the communication signal generates a bandwidth increase compared to the initial bandwidth of the FMCW waveform. This issue is analysed in [19], which separates the chirp in a three-section waveform to limit the excess bandwidth. To increase the data rate, the developed waveform is associated with Low Density Parity Check (LDPC) codes in [20]. Another solution proposed by [21] is to modify the rate of transmission during the chirp duration.

Yet, in automotive applications, interference between multiple RADAR or RADAR-communication systems remains a major issue with the constantly increasing number of vehicles (and consequently, of RADAR or RADAR-communication systems). This challenge has been tackled by the MOre Safety for All by Radar Interference Mitigation (MOSARIM) project [22]. Different interference mitigation techniques have been developed in [23]–[29], involving space, time, frequency, code and polarisation domains. However, even if dynamic parameters modifications are possible with RADAR systems, such solutions are suited for DFRC systems since communication receivers are not collocated with the transmitter and are unaware of these possible modifications. Other approaches for interference cancellation are detailed in [30]–[34], involving e.g. iterative cancellation or sparsity-based reconstruction.

In this paper, we consider Phase Coded (PC) FMCW DFRC systems as proposed in [7], [16]. With that kind of system,

François De Saint Moulin is a Research Fellow of the Fonds de la Recherche Scientifique - FNRS.

978-1-6654-8243-1/22/$31.00 ©2022 IEEE

Authorized licensed use limited to: Univ Catholique de Louvain/UCL. Downloaded on September 28,2022 at 09:57:20 UTC from IEEE Xplore. Restrictions apply.

the impact of interference on the RADAR and communication functions is studied, and the performance improvement achieved with cancellation at each function is analysed. Note that all investigated DFRC systems share the same parameters.

A. Contributions

The contributions of this paper are summarised as follows:

- The analysis of [7] regarding the impact of phase coding on the output SNR is extended to evaluate the impact of interference on the delay-Doppler map for the RADAR function; the impact of interference on the communication function is also briefly discussed.
- The improvements of detection probability and Bit Error Rate (BER) after interference cancellation at both functions are evaluated in specific scenarios.
- The involved power levels are analysed using stochastic geometry in a two-way road scenario in order to evaluate the relevance of the presented methods.

First, Section II summarises the basics of PC-FMCW DFRC. Then, Sections III and IV analyse the impact of correlated interference (systems with identical parameters) respectively on the RADAR and communication receivers. Additionally, the performance of interference cancellation on both functions in cooperation with the other function is studied. Finally, the power levels encountered in an automotive scenario with a two-way road are evaluated in Section V using stochastic geometry.

II. PC-FMCW DFRC

With an FMCW RADAR, multiple increasing or decreasing chirps are transmitted. Assuming that the transmission occurs in a frequency band $f \in [f_c - B/2, f_c + B/2]$ where f_c is the carrier frequency and B the bandwidth, if P pulses of duration T are transmitted with a PRI T_{PRI}, the instantaneous frequency of the transmitted signal is given by

$$f(t) = f_c + \sum_{p=0}^{P-1} \left[-\frac{B}{2} + \frac{B}{T}\left(t - pT_{\text{PRI}}\right) \right] \Pi\left(\frac{t - pT_{\text{PRI}}}{T}\right), \tag{1}$$

where Π is the (shifted) rectangular function, i.e. $\Pi(t) = 1$ if $t \in [0, 1]$. Note that $T_{\text{PRI}} \geq T$, allowing the insertion of a guard interval $T_g = T_{\text{PRI}} - T$ between successive pulses. The corresponding transmitted signal in baseband is given by

$$s(t) = \sum_{p=0}^{P-1} e^{-j\pi B(t - pT_{\text{PRI}})} e^{j\pi \frac{B}{T}(t - pT_{\text{PRI}})^2} \Pi\left(\frac{t - pT_{\text{PRI}}}{T}\right). \tag{2}$$

Let us consider a complex pulse modulation where symbols $\mathbf{I}$ are pulse shaped with a rectangular filter of width $T_c = T/L_c$, with L_c the number of transmitted symbols per pulse. In a PC-FMCW DFRC system, these symbols are modulated by a pulse train to form the following signal:

$$x(t) = \sum_{p=0}^{P-1} \sum_{l=0}^{L_c-1} I(l,p)\, \Pi\left(\frac{t - pT_{\text{PRI}} - lT_c}{T_c}\right) \cdot e^{-j\pi B(t - pT_{\text{PRI}})}\, e^{j\pi \frac{B}{T}(t - pT_{\text{PRI}})^2}\, \Pi\left(\frac{t - pT_{\text{PRI}}}{T}\right). \tag{3}$$

At the receiver, defining K targets at distances r_k and with radial speeds v_k, the received signal is obtained as follows:

$$r(t) = \sum_{k=0}^{K-1} \alpha_k\, e^{-j2\pi f_c \tau_k}\, e^{-j2\pi f_{\text{D}k} t} x\left(t - \tau_k\right) + w(t), \tag{4}$$

where α_k are the complex amplitudes, $\tau_k = 2r_k/c$ are the delays, $f_{\text{D}k} = 2v_k/c$ are the Doppler frequencies and w is an Additive White Gaussian Noise (AWGN).

A. RADAR receiver

At the RADAR receiver, the signal is dechirped by mixing it with the conjugate of the modulating chirps. Let us define the pulse notation of signal x as $x(t,p) = x\left(t + pT_{\text{PRI}}\right)$ with $t \in [0, T_{\text{PRI}}]$ and $p = 0, ..., P-1$. Assuming that $\tau_k \leq T_g \forall k$ (or equivalently that all high frequencies components generated at the start of the chirp by the previous pulse have been filtered), neglecting the noise for readibility, it follows that

$$y(t,p) = r(t,p)s^*(t,p) = \sum_{k=0}^{K-1} \sum_{l=0}^{L_c-1} I(l,p)\, \Pi\left(\frac{t - \tau_k - lT_c}{T_c}\right) \cdot \tilde{\alpha}_k\, e^{-j2\pi f_{\text{D}k} T_{\text{PRI}} p}\, e^{-j2\pi f_{\text{B}k} t}\, \Pi\left(\frac{t - \tau_k}{T - \tau_k}\right), \tag{5}$$

where $\tilde{\alpha}_k = \alpha e^{-j2\pi f_c \tau_k}\, e^{j\pi B \tau_k (1 + \tau_k/T)}$, and $f_{\text{B}k} = \tau_k B/T + f_{\text{D}k}$ is the beat frequency. If the communication symbols inserted in the waveform are not suppressed, the presence of random symbols induces a dispersion of the target's power in the delay-Doppler map (see Section III-A). However, the symbol pulses contained in the signal coming back from target k are delayed with an unknown delay τ_k. Still assuming that $f_{\text{B},k} \approx \tau_k B/T$, the beat frequency of each path is proportional to its delay. Therefore, the multiple copies of the communication signal can be aligned with the start of the chirp using a group delay filter $H_{\text{gd}}(f)$ with modulus and phase

$$|H_{\text{gd}}(f)| = 1, \quad \tau_{\text{gd}}(f) = \frac{T}{B} f \leftrightarrow \angle H_{\text{gd}}(f) = -\pi \frac{T}{B} f^2,$$

where τ_{gd} is the group delay of the filter. If the bandwidth of the communication signal component is small compared to the variation of the group delay around the beat frequency, the signal at the output of the group delay filter expressed in pulse notation is approximatively given by

$$y_{\text{gd}}(t,p) \approx \sum_{l=0}^{L_c-1} I(l,p)\, \Pi\left(\frac{t - lT_c}{T_c}\right) \cdot \sum_{k=0}^{K-1} \tilde{\alpha}_k\, e^{-j\pi \frac{T}{B} f_{\text{B}k}^2}\, e^{-j2\pi f_{\text{D}k} T_{\text{PRI}} p}\, e^{-j2\pi f_{\text{B}k} t}\, \Pi\left(\frac{t}{T - \tau_k}\right), \tag{6}$$

and the communication signal can be compensated to obtain the delay-Doppler map after sampling and applying a 2D-Discrete Fourier Transform (DFT). This map is typically fed to a detector (e.g. a Constant False Alarm Rate (CFAR) detector) in order to deduce the number of targets and their parameters.

Authorized licensed use limited to: Univ Catholique de Louvain/UCL. Downloaded on September 28,2022 at 09:57:20 UTC from IEEE Xplore. Restrictions apply.

B. Communication receiver

In a flat fading channel with attenuation and phase shift α_c, delay τ_c and Doppler frequency $f_{\mathrm{D}c}$, the start of the transmitted chirps must be detected in order to dechirp the received signal. Assuming a perfect time synchronisation, the communication signal is recovered without any artefact after dechirping:

$$r_{\mathrm{c}}(t) = \alpha_c e^{-j2\pi f_{\mathrm{D}c}(t+\tau_c)} \sum_{p=0}^{P-1} \sum_{l=0}^{L_c-1} I(l,p) \Pi \left(\frac{t - pT_{\mathrm{PRI}} - lT_c}{T_c} \right). \quad (7)$$

In that case, usual communication processing (matched filter, synchronisation and decision) can be applied to decode the transmitted symbols. The synchronisation algorithms used in this paper are the following: for the time synchronisation, a correlation is performed with the first pulse containing only pilots symbols. The carrier frequency offset is estimated by applying a DFT over pilots inserted at the same symbol indices in the successive pulses. Finally, the complex attenuation is estimated with a maximum likelihood estimator applied to the pilots of the first pulse.

With a frequency selective channel, owing to the multiple delays of the multipath components in the signal, asynchronous paths will experience increased frequency offsets and additional phase shifts after dechirping.

III. Interference on the RADAR function

Let us consider a scenario with one target and one interferer being another PC-FMCW DFRC system with the same parameters (f_c, T_{PRI}, T_{CPI}, B, T, and L_c).

A. Theoretical analysis

The interfering component is filtered at the RADAR receiver after dechirping if the generated beat frequency is higher than the cut-off frequency of the receiver low pass filter. However, if the relative delay between the interferer and the receiver is lower than the maximum unambiguous delay of the RADAR receiver, the delay-Doppler map is corrupted by the interferer. Fortunately, the transmitted data are different for the transmitter and the interferer, enabling an inherent interference mitigation. Let us consider the following signal in pulse notation and discrete time:

$$x_{\mathrm{I}}(n,p) = \alpha_{\mathrm{I}}\, e^{-j2\pi f_{\mathrm{DI}} T_{\mathrm{PRI}} p}\, e^{-j2\pi f_{\mathrm{BI}} T_s n} \cdot \sum_{l=0}^{L_c-1} I(l,p)\, \Pi_{\mathrm{D}}\left(n - lM, M\right), \quad (8)$$

with α_I a complex attenuation, f_{DI} a Doppler frequency, f_{BI} a beat frequency, M the number of samples per symbol, $T_s = T_c/M$ the sample period and where Π_{D} is the discrete rectangular function, i.e. $\Pi_{\mathrm{D}}(n, M) = 1$ for $n = 0, ..., M-1$. This signal represents either an interfering signal from another PC-FMCW DFRC system or a RADAR echo from which the communication symbols have not been suppressed. Assuming independent symbols of variance σ_I^2, and a path attenuation of variance $\sigma_{\alpha_{\mathrm{I}}}^2$, the expectation of the auto-correlation of x_{I} is given by

$$\begin{aligned}\Gamma_{x_{\mathrm{I}}}(\Delta_n, \Delta_p) &= \mathbb{E}\left[\sum_{p=0}^{P-1} \sum_{n=0}^{ML_c-1} x_{\mathrm{I}}(n,p)\, x_{\mathrm{I}}^*(n-\Delta_n, p-\Delta_p) \right] \\ &= \sigma_{\alpha_{\mathrm{I}}}^2\, \sigma_I^2\, P\, \delta(\Delta_p)\, e^{-j2\pi f_{\mathrm{B}} T_s \Delta_n}\, C_{\Pi}(\Delta_n), \end{aligned} \quad (9)$$

with

$$C_{\Pi}(k) = \sum_{l=0}^{L_c-1} \sum_{n=0}^{ML_c-1} \Pi_{\mathrm{D}}\left(n - lM, M\right) \Pi_{\mathrm{D}}\left(n - k - lM, M\right).$$

Applying a 2D-DFT to $\Gamma_{x_{\mathrm{I}}}$ provides an insight of the power dispersion of the signal into the delay-Doppler domain:

$$\mathcal{P}_{x_{\mathrm{I}}}(a,b) = \sigma_{\alpha_{\mathrm{I}}}^2\, \sigma_I^2\, PL_c\, \frac{\sin^2(\pi(a + f_{\mathrm{B}} T_s M L_c)/L_c)}{\sin^2(\pi(a + f_{\mathrm{B}} T_s M L_c)/ML_c)}. \quad (10)$$

This can be compared to the power distribution of a RADAR echo in which the communication symbols have been compensated. In that case, let us define

$$x(n,p) = \alpha\, e^{-j2\pi f_{\mathrm{D}} T_{\mathrm{PRI}} p}\, e^{-j2\pi f_{\mathrm{B}} T_s n}, \quad (11)$$

with α a complex attenuation, f_{D} a Doppler frequency and f_{B} a beat frequency. The power dispersion in the delay-Doppler domain is obtained as

$$\mathcal{P}_x(a,b) = \sigma_\alpha^2 \frac{\sin^2(\pi(a + f_{\mathrm{B}} T_s M L_c))}{\sin^2(\pi(a + f_{\mathrm{B}} T_s M L_c)/ML_c)} \frac{\sin^2(\pi(b + f_{\mathrm{D}} T_{\mathrm{CPI}}))}{\sin^2(\pi(b + f_{\mathrm{B}} T_{\mathrm{CPI}})/P)}. \quad (12)$$

When the data are compensated, (12) shows that peaks of amplitude $\sigma_\alpha^2\, P^2\, M^2\, L_c^2$ appear in the power spectrum map, centered around the beat and Doppler frequencies to estimate the target parameters. However, when data are not compensated, (10) shows that the power of each peak is uniformly spread in the Doppler dimension, and a sinc shape appears in the delay dimension. The main lobe width is proportional to L_c, and the peak amplitude is $\sigma_{\alpha_{\mathrm{I}}}^2\, \sigma_I^2\, P\, M^2\, L_c$. Therefore, assuming normalised symbols and the same path attenuation ($\sigma_\alpha^2 = \sigma_{\alpha_{\mathrm{I}}}^2$), an SNR gain of $10\log_{10}(PL_c)$dB is observed in the delay-Doppler map between the peak amplitude generated by the echoes and the peak amplitude generated by interfering signals thanks to the coding of the FMCW waveform. However, the interfering power is spread on the delay-Doppler domain and is not suppressed, leading to an increased noise floor.

B. Interference cancellation

Usually, the power of the communication signal is assumed to be larger than the power of the RADAR echoes. Therefore, interference cancellation can be applied: the communication signal is decoded by the communication receiver, and the information (transmitted symbols and synchronisation parameters) obtained in that way are transferred to the RADAR receiver to cancel interference. The receiver is illustrated in Figure 1. In order to evaluate the performance, an arbitrary scenario is defined, leading to parameters presented in Table I.

Authorized licensed use limited to: Univ Catholique de Louvain/UCL. Downloaded on September 28,2022 at 09:57:20 UTC from IEEE Xplore. Restrictions apply.

TABLE I
SIMULATION PARAMETERS FOR INTERFERENCE CANCELLATION AT THE RADAR RECEIVER.

B = 20MHz	T = 100μs	T_g = 5μs
P = 50	L_c = 100	K = 2
$\lvert\alpha_{0-1}\rvert$ = 0.1/0.1	τ_{0-1} = 1/3μs	$f_{\mathrm{D}0-1}$ = 1000/-500Hz
$\lvert\alpha_c\rvert$ = 1	τ_c = 2.5μs	$f_{\mathrm{D}c}$ = -300Hz

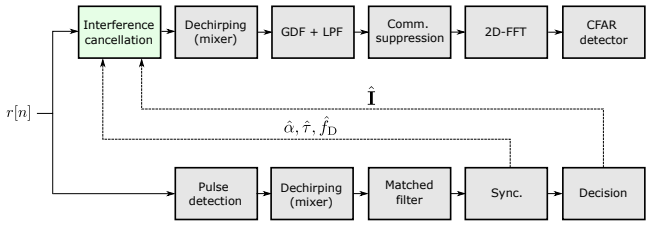


Fig. 1. Receiver chain with interference cancellation at the RADAR receiver. The communication receiver forwards estimates of the attenuation, phase shift, delay, Doppler frequency and decoded symbols to the RADAR receiver.

Figure 2 illustrates the probability of detection obtained for different modulation indices (BPSK, QPSK and 16-QAM) after interference cancellation at the RADAR receiver, compared to the probability of detection obtained when there is no interference, or when interference is not cancelled. Note that the interference level is similar for every modulation index when there is no cancellation since the constellations are normalised. In the considered scenario, the communication signal power is 20dB higher than RADAR echoes. Even if the interference power is spread in the delay-Doppler map owing to the presence of uncompensated communication symbols, the RADAR echoes are hidden by the interference. However, the interference induced by the RADAR echoes on the communication receiver is limited, enabling the communication function to perform correctly. The BER obtained at the communication receiver for different modulation indices (BPSK, QPSK and 16-QAM) is shown in Figure 3. At low SNR, the BER is high, leading to multiple symbol errors at the cancellation. The higher the modulation index, the higher the number of errors, leading to a decrease of the probability of detection. In that case, the obtained performance is even worse than the performance obtained when there is no interference cancellation with high modulation indices. However, at higher SNR, the BER decreases, and the cancellation efficiency increases as well. Therefore, the probability of detection increases to one. The increase is slower for high modulation indices since the BER decreases more slowly in the considered SNR range.

C. Summary

When the communication component is dominant compared to the RADAR echoes, interference cancellation performs well when the BER obtained at the communication output is sufficiently low. The modulation index of the communication signal can be increased at the price of a lower detection probability for a given SNR at the communication function.

IV. INTERFERENCE ON THE COMMUNICATION RECEIVER

Let us assume again that every PC-FMCW DFRC system shares the same parameters.

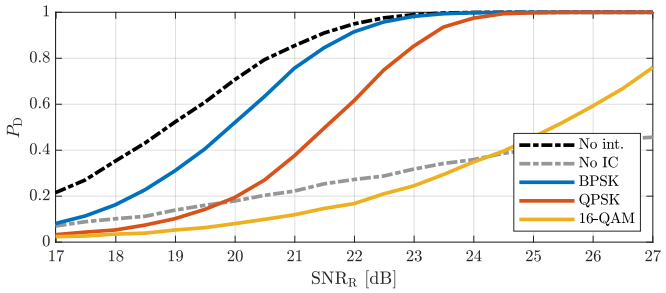


Fig. 2. Probability of detection against RADAR SNR with BPSK, QPSK and 16-QAM modulation, before and after Interference Cancellation (IC), with false alarm probability $P_{\mathrm{FA}} = 10^{-4}$. The RADAR SNR is defined as $\mathrm{SNR_R} = PL_c\ \mathrm{SNR_C}\ |\alpha_0|^2/|\alpha_c|^2$ where $\mathrm{SNR_C}$ is the communication SNR. Note that no interference is included in the RADAR and communication SNRs.

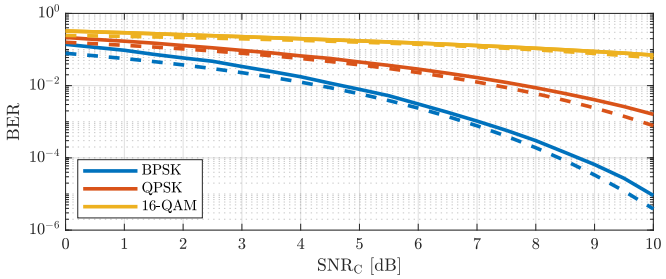


Fig. 3. BER against communication SNR with BPSK, QPSK and 16-QAM modulation, in theory (dashed lines) and in simulation (solid lines).

A. Theoretical analysis

As for the RADAR receiver, dechirping is applied at the communication receiver. Hence, the interfering components rotate owing to the inherent Doppler frequencies of the paths and the generated beat frequencies. Since the DFRC parameters are considered to be the same for every system, there is no inherent interference mitigation in the receiver. Therefore, interference cancellation must be applied to increase the communication performance if interference occurs.

The interference is either generated from other DFRC systems, or it arises from the DFRC system itself (named *self-interference* in this paper): since both functions are collocated, the RADAR echoes will interfere with the communication receiver. Usually, it is assumed that the power of the RADAR echoes is negligible compared to the power of the communication signal. However, in some specific scenarios, the opposite can occur, motivating an analysis of the achieved performance in that case.

B. Interference cancellation

With self-interference, the transmitter forwards the symbols of the emitted signal to the communication receiver in order to suppress the RADAR echoes. Additionally, the outputs of the RADAR receiver (the number of echoes, their delays and their Doppler frequencies) are also forwarded, such that the attenuation and phase shift are the only parameters to estimate for the cancellation. This system is illustrated in Figure 4. Another option is to estimate all the parameters of each RADAR echo successively based on the estimated number of targets of the RADAR receiver, instead of using RADAR

Authorized licensed use limited to: Univ Catholique de Louvain/UCL. Downloaded on September 28,2022 at 09:57:20 UTC from IEEE Xplore. Restrictions apply.

estimates of the echoes' delay and Doppler frequencies. With interference coming from another DFRC system, the interfering signal must be decoded to recover the transmitted symbols, and the synchronisation parameters must all be estimated at the communication receiver. In this paper, self-interference only is considered in order to be able to compare the performance of the interference cancellation either when the RADAR outputs are forwarded or with an additional estimation of the echoes parameters at the communication function. Another scenario has been defined to evaluate the performance of the system with interference cancellation at the communication function, leading to parameters presented in Table II.

TABLE II
SIMULATION PARAMETERS FOR INTERFERENCE CANCELLATION AT THE COMMUNICATION RECEIVER.

B = 20MHz	T = 100μs	T_g = 5μs
P = 50/100/180/200	L_c = 100	K = 2
$\lvert\alpha_{0-2}\rvert$ = 1/0.8/0.5	τ_{0-2} = 1/3/4μs	$f_{\mathrm{D}0-2}$ = 1000/-500/300Hz
$\lvert\alpha_c\rvert$ = 1	τ_c = 2.5μs	$f_{\mathrm{D}c}$ = -300Hz

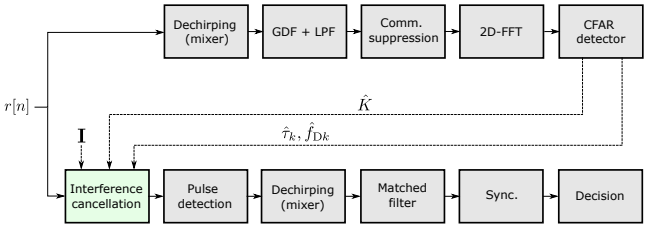


Fig. 4. Receiver chain with interference cancellation at the communication receiver. The RADAR receiver forwards the transmitted symbols and estimates of the number of targets, their delays and their Doppler frequencies.

Figure 5 illustrates the BER obtained with one target for different false alarm probabilities and pulse numbers. When the delay and Doppler frequency estimations are based on the RADAR receiver output, the achieved performance depends on the precision of the RADAR estimates, which are directly related to the delay and Doppler resolutions requirements. With the parameters given in Table II, the Doppler resolutions are respectively equal to 190Hz, 95Hz, 53Hz, and 48Hz with 50, 100, 180 and 200 pulses. Improving the resolution leads to better performance when it enables to improve the estimation, e.g. when 180 pulses are transmitted. However, this also increases the duration of the payload, leading to more errors at the end of the payload when the Doppler frequency estimation is not sufficiently accurate. For instance, in the scenario depicted in Table II, when 100 pulses are transmitted, the Doppler resolution is higher but the estimation error is the same compared to when 50 pulses are transmitted and the payload length is doubled, leading to worse performance. In contrary, with 200 pulses, the estimation of the Doppler frequency is very accurate and the achieved performance reaches the theoretical curve. Finally, the BER slightly increases with the false alarm probability. Indeed, false alarms induce the cancellation of non existing signal components, which is translated by an increase of the interference level.

Another solution is to use the synchronisation algorithms of the communication receiver on the RADAR echoes to estimate

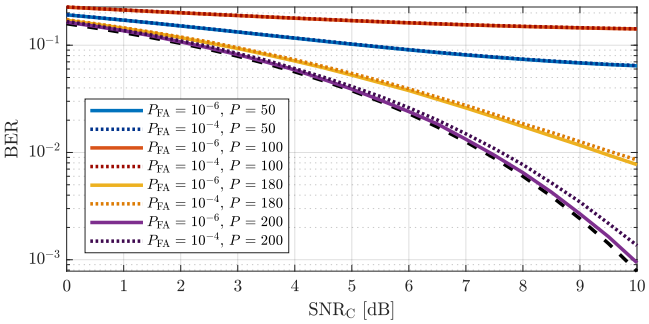


Fig. 5. BER against communication SNR for multiple false alarm probabilities and pulse numbers with one target and QPSK symbols. The RADAR estimates of the delays and Doppler frequencies are forwarded to the communication receiver. The dashed curve represents the achieved BER without any interference.

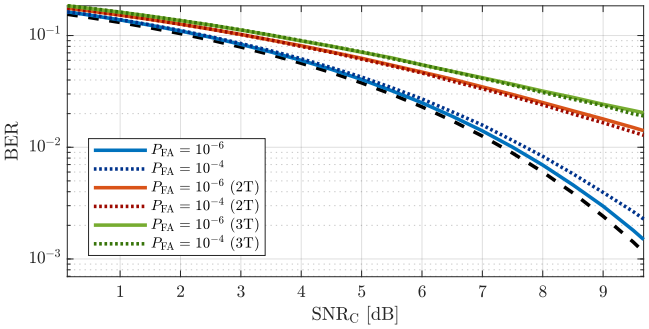


Fig. 6. BER against communication SNR for multiple false alarm probabilities and number of targets with QPSK symbols. The synchronisation algorithm of the communication receiver are applied to the RADAR echoes. The dashed curve represents the achieved BER without any interference.

their delays, Doppler frequencies, complex attenuations, at the price of additional processing. Figure 6 illustrates the BER obtained in that case, with one to three targets and for different false alarm probabilities. With one target, the performance is close to the case without interferer, and comparable to the performance achieved in Figure 5 when 200 pulses are transmitted. When the number of RADAR echoes is increased, the performance decreases. In the considered scenario in Table II, the second and third RADAR echoes have an amplitude lower than the amplitude of the communication signal. Therefore, the communication signal induces errors in the estimation of the complex attenuation of the RADAR echoes, leading to a worse interference cancellation. Note that a lower false alarm probability leads to better performance with two and three targets: since the synchronisation algorithm of the communication receiver is applied on the RADAR echoes, the only parameter transferred from the RADAR receiver is the estimated number of targets. Therefore, thanks to false alarms, an echo which has not been efficiently cancelled is suppressed multiple times. However, there is still performance degradations when all the echoes have been efficiently cancelled.

C. Summary

When the RADAR echoes are dominant compared to the communication signal, interference cancellation can be applied efficiently to the communication receiver to cancel the RADAR echoes. The estimation of the echoes' parameters is either

Authorized licensed use limited to: Univ Catholique de Louvain/UCL. Downloaded on September 28,2022 at 09:57:20 UTC from IEEE Xplore. Restrictions apply.

based on the RADAR outputs, or on the communication synchronisation algorithm. In the former, the RADAR delay and Doppler resolutions should be sufficient in order to ensure accurate estimations of the delays and Doppler frequencies and an efficient cancellation. However, the performance decreases with the number of echoes to suppress.

V. Relative Power Levels

The performance of interference cancellation at both functions are closely related to the scenario through the relative power levels between the RADAR echoes and the communication signal. In order to evaluate this power ratio, the scenario illustrated in Figure 7 is considered.

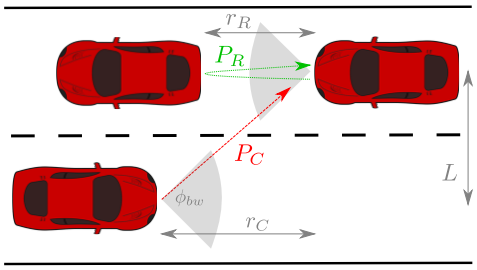


Fig. 7. Two-lanes road scenario.

On a two-lanes road with width L, all vehicles are supposed to have a RADAR Cross Section (RCS) σ and are equipped at the front with the same DFRC system using identical parameters. The vehicle of interest receives a RADAR echo coming from the first vehicle driving ahead, while a communication signal is received from the closest vehicle driving in the opposite lane. The transmit and receive antennas have an antenna beamwidth ϕ_{bw}. The vehicles are distributed on each lane following two independent 1D Poisson Point Processes (PPP) of densities $\lambda_R(r)$ and $\lambda_C(r)$, where $\lambda_R(r) = \lambda \mathbb{1}(r_{R\text{min}} \leq r < r_{R\text{max}})$ and $\lambda_C(r) = \lambda \mathbb{1}(r_{C\text{min}} \leq r)$, with λ the vehicles density, $\mathbb{1}$ the indicator function, $r_{R\text{min}}$ (resp. $r_{C\text{min}}$) the minimum distance for the closest vehicle in the opposite lane (resp. in the same lane) and $r_{R\text{max}}$ the maximum RADAR detectable range. While $r_{R\text{min}}$ is chosen arbitrarily as the minimum distance between two vehicles in the considered scenario, $r_{C\text{min}}$ is directly related to the antenna beamwidth and lane width: $\tan(\phi_{bw}/2) = L/r_{C\text{min}}$. Based on the void probability of PPPs, the Probability Density Functions (PDF) of the closest vehicles in each lane are obtained as

$$f_{r_R}(r) = \frac{\lambda\, e^{-\lambda(r-r_{R\text{min}})}}{1 - e^{-\lambda(r_{R\text{max}}-r_{R\text{min}})}}\, \mathbb{1}(r_{R\text{min}} \leq r < r_{R\text{max}}). \quad (13)$$

and

$$f_{r_C}(r) = \lambda\, e^{-\lambda(r-r_{C\text{min}})}\, \mathbb{1}(r_{C\text{min}} \leq r). \quad (14)$$

Let us consider a linear path-loss model $L\,[\text{dB}] = \beta\,[\text{dB}] + 10\alpha \log_{10}(r)$ where α is the path-loss exponent and β is the floating intercept. Following the RADAR equation [35], [36], the received power for the RADAR echoes with a target at a distance r_R is given by

$$P_R = P_T G_T G_R \frac{c^2}{4\pi f_c^2}\, \beta^{-2} r_\text{R}^{-2\alpha}\, \sigma, \quad (15)$$

where P_T is the transmit power, G_T and G_R are respectively the transmit and receive antenna gains, f_c is the carrier frequency and c is the speed of light. The received power of the communication signal at a distance r_C (in the road direction) is given by the Friis equation as

$$P_C = P_T G_T G_R \frac{c^2}{4\pi f_c^2}\, \beta^{-1} \left(r_\text{C}^2 + L^2\right)^{-\frac{\alpha}{2}}. \quad (16)$$

Therefore, the power ratio between the RADAR and the communication signal is given by

$$\eta(r_R, r_C) = \frac{P_R}{P_C} = \frac{\sigma}{\beta} \left(\frac{\sqrt{r_\text{C}^2 + L^2}}{r_\text{R}^2}\right)^{\alpha}. \quad (17)$$

The Cumulative Distribution Function (CDF) of the power ratio is then obtained as

$$F_\eta(x) = \int_0^\infty \int_0^\infty \mathbb{1}(\eta(r_R, r_C) \leq x)\, f_{r_R}(r_R) f_{r_C}(r_C) \mathrm{d}r_R \mathrm{d}r_C. \quad (18)$$

The amplitude ratio between the RADAR and the communication signal can also be computed in the same way.

TABLE III
Simulation Parameters for the Two-Lanes Road Scenario.

$\sigma = 100\text{m}^2$	$L = 3\text{m}$	$\phi_{\text{bw}} = 60°$
$r_{R\text{min}} = 5\text{m}$	$\lambda = 10^{-1}\text{m}^{-1}$	$\alpha = 2, \beta = 4\pi$

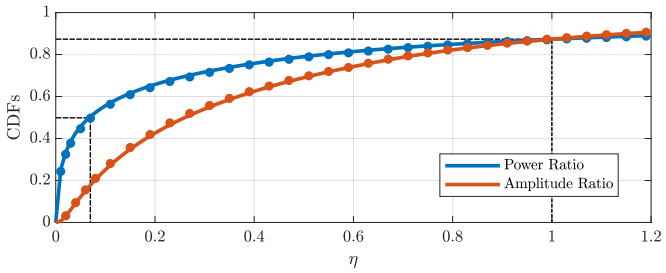


Fig. 8. CDF of the power and amplitude ratio. Continuous and dots are respectively computed with stochastic geometry and Monte-Carlo simulations.

Figure 8 shows the CDF of the power and amplitude ratio obtained with parameters described in Table III. In nearly ninety percent of the scenarios, a smaller power is received for the RADAR echo compared to the communication signal. Additionally, in 50% of the cases, the communication signal power is at least 10dB higher than the RADAR echo power. This suggests to apply interference cancellation at the RADAR receiver rather than at the communication receiver.

VI. Conclusion

Interference between multiple DFRC systems is a major issue for the future, especially for automotive scenarios. While an inherent interference mitigation is present at the RADAR receiver thanks to the introduction of communication symbols, there is no inherent mitigation at the communication receiver. In order to improve the performance, interference mitigation must be introduced at the RADAR or communication receiver depending on the scenario. For a two-way automotive scenario, it has been shown with stochastic geometry that the communication signal power is larger than the RADAR echo power

Authorized licensed use limited to: Univ Catholique de Louvain/UCL. Downloaded on September 28,2022 at 09:57:20 UTC from IEEE Xplore. Restrictions apply.

in most cases. Therefore, interference cancellation should be applied at the RADAR receiver.

In future research, an estimation of the signal power levels should be designed in order to activate or deactivate interference cancellation at the RADAR and communication receiver, such that all situations can be handled. Otherwise, improvements of the RADAR estimates based on previous measurements should be investigated. Finally, stochastic geometry could be used to further analyse trade-offs between the RADAR and communication functions.

REFERENCES

[1] L. Zheng, M. Lops, Y. C. Eldar, and X. Wang, "Radar and Communication Co-existence: an Overview," 2019.

[2] F. Liu, C. Masouros, and S. Member, "A Tutorial on Joint Radar and Communication Transmission for Vehicular Networks - Part I : Background and Fundamentals," vol. 7798, no. c, pp. 3–7, 2020.

[3] N. C. Luong, X. Lu, D. T. Hoang, D. Niyato, and D. I. Kim, "Radio Resource Management in Joint Radar and Communication: A Comprehensive Survey," *IEEE Communications Surveys and Tutorials*, vol. 23, no. 2, pp. 780–814, 2021.

[4] J. Mietzner and A. Santra, "Space-Time Waveform Coding for Joint Radar and Wireless Communications (RadCom) Applications," *IEEE Wireless Communications and Networking Conference, WCNC*, vol. 2020-May, 2020.

[5] P. Barrenechea, F. Elferink, and J. Janssen, "FMCW radar with broadband communication capability," *2007 European Radar Conference, EURAD*, no. October, pp. 130–133, 2007.

[6] M. B. Alabd, B. Nuss, C. Winkler, and T. Zwick, "Partial chirp modulation technique for chirp sequence based radar communications," *EuRAD 2019 - 2019 16th European Radar Conference*, pp. 173–176, 2019.

[7] F. Uysal, "Phase-Coded FMCW automotive radar: System design and interference mitigation," *IEEE Transactions on Vehicular Technology*, vol. 69, no. 1, pp. 270–281, 2020.

[8] A. N. Barreto, T. M. Pham, S. George, P. Sen, and G. Fettweis, "Analysis of a Chirp-Based Waveform for Joint Communications and Radar Sensing (JCS) using Non-Linear Components," *15th European Conference on Antennas and Propagation, EuCAP 2021*, 2021.

[9] M. Bekar, C. J. Baker, E. G. Hoare, and M. Gashinova, "Joint MIMO Radar and Communication System Using a PSK-LFM Waveform with TDM and CDM Approaches," *IEEE Sensors Journal*, vol. 21, no. 5, pp. 6115–6124, 2021.

[10] P. M. McCormick, C. Sahin, S. D. Blunt, and J. G. Metcalf, "FMCW implementation of phase-attached radar-communications (PARC)," *2019 IEEE Radar Conference, RadarConf 2019*, pp. 0–5, 2019.

[11] F. Uysal and S. Orru, "Phase-coded FMCW automotive radar: Application and challenges," *2020 IEEE International Radar Conference, RADAR 2020*, no. 4, pp. 478–482, 2020.

[12] U. Kumbul, N. Petrov, F. Van Der Zwan, C. S. Vaucher, and A. Yarovoy, "Experimental Investigation of Phase Coded FMCW for Sensing and Communications," *15th European Conference on Antennas and Propagation, EuCAP 2021*, 2021.

[13] D. Ma, T. Huang, N. Shlezinger, Y. Liu, X. Wang, and Y. C. Eldar, "A DFRC System Based on Multi-Carrier Agile FMCW MIMO Radar for Vehicular Applications," *2020 IEEE International Conference on Communications Workshops, ICC Workshops 2020 - Proceedings*, 2020.

[14] D. Ma, N. Shlezinger, T. Huang, Y. Liu, and Y. C. Eldar, "FRaC: FMCW-Based Joint Radar-Communications System via Index Modulation," no. 646804, pp. 1–16, 2021.

[15] Z. Dou, X. Zhong, and W. Zhang, "Radar-Communication Integration Based on MSK-LFM Spread Spectrum Signal," *International Journal of Communications, Network and System Sciences*, vol. 10, no. 08, pp. 108–117, 2017.

[16] F. Lampel, R. F. Tigrek, A. Alvarado, and F. M. Willems, "A performance enhancement technique for a joint FMCW radcom system," *EuRAD 2019 - 2019 16th European Radar Conference*, pp. 169–172, 2019.

[17] H. Bao, A. Ziemann, and Z. S. He, "Design and Measurements of MSK-LFM RadCom System," *EuRAD 2020 - 2020 17th European Radar Conference*, no. January, pp. 9–12, 2021.

[18] Y. Zhang, Q. Li, L. Huang, and J. Song, "Waveform design for joint radar-communication system with multi-user based on MIMO radar," *2017 IEEE Radar Conference, RadarConf 2017*, pp. 0415–0418, 2017.

[19] Y. Zhang, Q. Li, L. Huang, K. Dai, and J. Song, "Waveform design for joint radar-communication with nonideal power amplifier and outband interference," *IEEE Wireless Communications and Networking Conference, WCNC*, pp. 0–5, 2017.

[20] Q. Li, K. Dai, Y. Zhang, and H. Zhang, "Integrated Waveform for a Joint Radar-Communication System with High-Speed Transmission," *IEEE Wireless Communications Letters*, vol. 8, no. 4, pp. 1208–1211, 2019.

[21] Y. Ni, Z. Wang, Q. Huang, and M. Zhang, "High Throughput Rate-Shift Integrated System for Joint Radar-Communications," *IEEE Access*, vol. 7, pp. 78228–78238, 2019.

[22] "More safety for all by radar interference mitigation (mosarim)," 2010. [Online] Available: https://cordis.europa.eu/project/rcn/94234/reporting/en.

[23] M. Rameez, M. Dahl, and M. I. Pettersson, "Adaptive digital beamforming for interference suppression in automotive FMCW radars," *2018 IEEE Radar Conference, RadarConf 2018*, pp. 252–256, 2018.

[24] Z. Slavik and K. V. Mishra, "Cognitive interference mitigation in automotive radars," *2019 IEEE Radar Conference, RadarConf 2019*, pp. 0–5, 2019.

[25] Y. Kitsukawa, M. Mitsumoto, H. Mizutani, N. Fukui, and C. Miyazaki, "An interference suppression method by transmission chirp waveform with random repetition interval in fast-chirp FMCW radar," *EuRAD 2019 - 2019 16th European Radar Conference*, pp. 165–168, 2019.

[26] Y. Kim, "Identification of FMCW radar in mutual interference environments using frequency ramp modulation," *2016 10th European Conference on Antennas and Propagation, EuCAP 2016*, pp. 11–13, 2016.

[27] S. Ishikawa, M. Kurosawa, M. Umehira, X. Wang, S. Takeda, and H. Kuroda, "Packet-based FMCW Radar using CSMA Technique to Avoid Narrowband Interefrence," *2019 International Radar Conference, RADAR 2019*, 2019.

[28] C. Aydogdu, M. F. Keskin, N. Garcia, H. Wymeersch, and D. W. Bliss, "Radchat: spectrum sharing for automotive radar interference mitigation," *arXiv*, pp. 1–14, 2019.

[29] S. Jin and S. Roy, "FMCW Radar Network: Multiple Access and Interference Mitigation," *IEEE Journal on Selected Topics in Signal Processing*, vol. 15, no. 4, pp. 968–979, 2021.

[30] M. Umehira, T. Nozawa, Y. Makino, X. Wang, S. Takeda, and H. Kuroda, "A novel iterative inter-radar interference reduction scheme for densely deployed automotive FMCW radars," *Proceedings International Radar Symposium*, vol. 2018-June, pp. 1–10, 2018.

[31] Z. Yang-Ping and Z. Zhu, "Linear frequency modulation interference suppression based on subspace error correction," *ICEIEC 2019 - Proceedings of 2019 IEEE 9th International Conference on Electronics Information and Emergency Communication*, no. 1, pp. 611–615, 2019.

[32] A. Correas-Serrano and M. A. Gonzalez-Huici, "Sparse reconstruction of chirplets for automotive FMCW radar interference mitigation," *2019 IEEE MTT-S International Conference on Microwaves for Intelligent Mobility, ICMIM 2019*, pp. 4–7, 2019.

[33] S. Neemat, O. Krasnov, and A. Yarovoy, "An interference mitigation technique for FMCW radar using beat-frequencies interpolation in the STFT domain," *IEEE Transactions on Microwave Theory and Techniques*, vol. 67, no. 3, pp. 1207–1220, 2019.

[34] Z. Liu, W. Lu, J. Wu, S. Yang, and G. Li, "A PELT-KCN Algorithm for FMCW Radar Interference Suppression Based on Signal Reconstruction," *IEEE Access*, vol. 8, pp. 45108–45118, 2020.

[35] A. Munari, L. Simic, and M. Petrova, "Stochastic geometry interference analysis of radar network performance," *IEEE Communications Letters*, vol. 22, no. 11, pp. 2362–2365, 2018.

[36] A. Al-Hourani, R. J. Evans, S. Kandeepan, B. Moran, and H. Eltom, "Stochastic Geometry Methods for Modeling Automotive Radar Interference," *IEEE Transactions on Intelligent Transportation Systems*, vol. 19, no. 2, pp. 333–344, 2018.

Authorized licensed use limited to: Univ Catholique de Louvain/UCL. Downloaded on September 28,2022 at 09:57:20 UTC from IEEE Xplore. Restrictions apply.